

# Stellar populations in blue compact galaxies

X. Kong<sup>1,3</sup> and F. Z. Cheng<sup>1,2</sup>

<sup>1</sup> Center for Astrophysics, University of Science and Technology of China, 230026, Hefei, P. R. China,

<sup>2</sup> National Astronomical Observatories, Chinese Academy of Sciences, 100012, Beijing, P. R. China,

<sup>3</sup> Beijing Astrophysics Center (BAC)<sup>†</sup>, 100871, Beijing, P. R. China

Received 28 May 1999 / Accepted 29 Sept. 1999

**Abstract.** Blue compact galaxies (BCGs) are compact galaxies that are dominated by intense star formation. Comparing the observational properties with the predictions of stellar population synthesis model, we have analyzed the nuclear stellar population and emission line spectra in a sample of 10 BCGs. The results indicate that the continuum flux fractions at 5870Å due to old stellar components and young stellar components are both important. The contribution from intermediate age components is different in different galaxies. Our results suggest that BCGs are old galaxies, in which star formation occurs in short intense burst separated by long quiescent phases. We have also derived the internal reddening for the stellar population by population synthesis method, and the internal reddening for the emitting gas clouds by the Balmer line ratio. The former is significantly smaller than the latter for BCGs. A model of clumpy foreground dust, with different covering factors for the gas and stars, can explain the difference. Combining the internal reddening value and the stellar population, we have decreased the effecting from the internal reddening and underlying stellar absorption, and accurately measured most emission lines for each BCGs. Using these emission lines, we have attempted to identify the ionizing mechanism of BCGs. The ionizing mechanism for these emission line regions of BCGs is typical of photoionization by stars, characteristics of a low extinction HII regions.

**Key words:** galaxies: abundances – galaxies: compact – galaxies: star clusters – galaxies: formation – galaxies: stellar content

## 1. Introduction

Blue compact galaxies (BCGs) were first observed spectroscopically by Sargent & Searle (1970), who clearly established that the properties of these galaxies implied high star formation rates at low metallicities (Doublier et al.

1997). BCGs have been thought to represent a different and extreme environment for star formation compared to the Milky Way and many other nearby galaxies. They are very important for understanding the star formation process and galactic evolution (Kinney et al. 1993, Martin 1998). BCGs are characterized by their compact morphology and very blue UVB colors (Sage et al. 1992, Hunter & Thronson 1995). Their optical spectra show strong narrow emission lines superposed on a nearly featureless continuum, similar to the spectrum of HII regions (Izotov et al. 1997, Östlin et al. 1999). Radio observations at 21-cm have shown BCGs contain large amounts of neutral hydrogen. The mean value of  $M_{\text{HI}}/M_{\text{tot}}$  for a sample of 122 BCGs is 0.16 (Krüger et al. 1995, Salzer & Norton 1999). Systematic spectroscopic studies of BCGs have shown that about one-third of BCGs have broad W-R bumps, mainly at  $\lambda 4650$  that are characteristic of late WN stars (Conti 1991, Izotov et al. 1997).

Ever since their discovery, the question has arisen whether BCGs are truly young systems where star formation is occurring for the first time, or whether they are old galaxies with current starburst superposed on an old underlying stellar population (Garnett et al. 1997, Lipovetsky et al. 1999). Because the star formation rate in BCGs is very high, the metallicity could have reached the observed value even within a time  $T \sim 10^8$ yr (Fanelli et al. 1988). Hence, one interpretation for the low metallicity, high gas content and high star formation rate is that BCGs are young objects, and they are being seen at the epoch of the formation of the first generation stars ( $T \sim 10^8$ yr). The other interpretation is that they are old objects in which star formation occurs in short bursts with long quiescent phases in between (Krüger et al. 1995, Gondhalekar et al. 1998, Östlin et al. 1999).

The low metal abundance together with the high star formation rates and large gas masses makes BCGs most suitable to determine the element abundance (Thuan et al. 1995, 1996), the primordial helium abundance  $Y_p$  (Izotov et al. 1994) and to study the variations of one chemical element relative to another (van Zee et al. 1998). It also provides a wealth of diagnostics for the study of intrinsic physical conditions (Izotov & Thuan 1999). The re-

Send offprint requests to: X. Kong (xkong@mail.ustc.edu.cn)

<sup>†</sup> BAC is jointly sponsored by the Chinese Academy of Sciences and Peking University.

sults of these papers are based on direct measurements of the emission line intensities, but according to Vaceli et al. (1997), the observed emission line intensities are affected by the underlying stellar absorption. Since the stellar absorption can affect substantially some fundamental emission lines used for the derivation of reddening and other physical and chemical properties, one of the first and most critical steps in the analysis of BCG spectroscopic properties is to quantify and remove the contribution of the stellar population.

If we can resolve the stellar population of a BCG, we can know its age and star formation regime. We can then subtract the stellar absorption line from the emission-line spectrum. With the launch of HST and 10-m class telescope, we are now witnessing a new era that allows to analyze in detail nearby objects, such as Galactic HII regions or 30 Dor in the LMC and resolve old red giants in a few distant galaxies (Grebel 1999). Such studies allow us to resolve and study individual stars in massive star clusters. However, as one studies objects at larger distances, individual stars (except for some giants) are unresolved and hence we are limited to studying their global properties (Mas-Hesse & Kunth 1998). In this paper we have selected 10 BCGs and determined their stellar population by applying a population synthesis method based on star cluster integrated spectra. In a subsequent paper, we will apply an evolution population synthesis method to these galaxies and the results of the two papers will be considered together.

The outline of the paper is as follows. In Sect. 2 we describe the observations and data reduction. In Sect. 3 we present measurements of equivalent widths and continuum analysis for the BCG spectra. In Sect. 4 we carry out the population synthesis and give the results of computation. In Sect. 5 we subtract the stellar population synthesis spectra from the observed ones and study the resulting emission line spectra. The results are presented in Sect. 6. In Sect. 7, we summarize our conclusions. Throughout this paper, we use a Hubble constant of  $H_0 = 50 \text{ km s}^{-1} \text{ Mpc}^{-1}$ .

## 2. Observations and Data Reduction

Our sample of 10 blue compact galaxies was selected from Kinney et al. 1993; seven of these have  $M_B > -20$  mag and are dwarf galaxies (BCDG). Table 1 describes the sample properties. The target names are listed in Column 1. Column 2 to Column 8 respectively give the source coordinates, morphological type, the radial velocity relative to the Local Group, photographic magnitude, absolute magnitude and Galactic reddening.

Long-slit spectroscopic observations were carried out in March and July of 1997. All the observations were made with the 2.16 m telescope at the Xinglong Station of Beijing Astronomical Observatory, using a Zeiss universal spectrograph with a grating of 300 grooves  $\text{mm}^{-1}$

dispersion. A Tek 1024×1024 CCD was employed, covering a spectral range from 3500 to 7500Å with a resolution of 9.6Å (2 pixels). The slit aperture was fixed at  $250\mu\text{m}$ , corresponding to  $2.5''$  projected on the sky, to match the typical seeing value at Xinglong Station, and is set at position angle  $90^\circ$ . All the spectra were extracted by adding the contributions of 5 pixels around the nucleus. The sky background was estimated from a linear interpolation of two regions located  $30''$  from the nucleus. The last two columns of Table 1 list the observation date and exposure time.

The standard reduction to flux units and transformation to linear wavelength scale were made using the IRAF<sup>1</sup> packages. The IRAF packages CCDRED, TWODSPEC and ONEDSPEC were used to reduce the long-slit spectral data. The wavelength was calibrated using a He/Ar comparison lamp. 20-odd lines were used to establish the wavelength scale, by fitting a first-order cubic spline. The accuracy of the wavelength calibration was better than 2Å. On most nights, more than two KPNO standard stars were used for relative flux calibration. We followed standard procedure in the data reduction: bias subtraction, flat fielding, sky subtraction, cosmic ray extinction, CCD response curve calibration, wavelength and photometric calibration, and extinction correction. The dark counts were so low that they were not subtracted. An estimate of the radial velocity of the galaxies was made to correct to zero red shift. The foreground reddening due to our Galaxy was corrected using the value from Burstein & Heiles (1984). Atmospheric extinction was corrected using the mean extinction coefficients for the Xinglong station. The final extracted spectra of the BCGs (labeled as OBS) are shown in Figure 1.

## 3. Measurements

Our main goal is to study the stellar population of BCGs. To do this, we have used the synthesis method described in Schmitt, Bica & Pastoriza (1996). The method minimizes the differences between the observed and synthetic equivalent widths for a set of spectral features. To measure the equivalent widths accurately, it is extremely important first to have a good fit to the continuum. Hence the analysis of each of the sample spectra proceeds in two steps (1) determining a pseudo-continuum at selected pivot-points, and (2) measuring the equivalent widths (EWs) for a set of selected spectral lines.

The continuum and EW measurements followed the method outlined in Bica & Alloin (1986), Bica (1988) and Bica et al. (1994), Cid Fernandes et al. (1998), and subsequently used in several studies of both normal and emission line galaxies (e.g., Jablonka et al. 1990, Storchi-Bergmann et al. 1995, McQuade et al. 1995, Bonatto et al. 1998). This method first determines a pseudo-continuum

<sup>1</sup> IRAF is provided by NOAO

**Table 1.** Parameters of the selected Blue Compact Galaxies and Log of optical observations

Galaxy Name	R.A. (B1950)	Decl. (B1950)	Morph.	$v_{\text{hel,obs}}$ km/s	$B_T$ (mag)	$M_B$ (mag)	$E(B-V)_G$	Obs. date dd/mm/yy	Exp. (sec.)
IC1586	00:45:17.0	22:06:07		5821	14.2	-20.53	0.02	25/07/1997	1500
NGC2537	08:09:42.5	46:08:32	Sc	441	12.4	-18.13	0.04	18/03/1997	1200
MRK19	09:12:53.5	59:58:53		4230	15.6	-19.07	0.03	18/03/1997	1800
MRK108	09:17:26.1	64:26:57	I0	1534	15.4	-17.57	0.04	18/03/1997	2000
MRK25	10:00:22.0	59:40:50		2602	14.8	-19.96	0.00	19/03/1997	1500
MRK35	10:42:16.5	56:13:23	Im	995	13.2	-18.50	0.00	18/03/1997	1200
NGC4194	12:11:41.7	54:48:21	Sm	2506	13.0	-20.71	0.00	19/03/1997	1500
UGC9560	14:48:55.1	35:46:36	Ir.	1213	14.8	-17.95	0.00	18/03/1997	1500
UGCA410	15:35:48.4	55:25:34	dE	665	15.4	-16.63	0.01	20/03/1997	2820
MRK499	16:47:02.6	48:47:44		7710	14.9	-21.12	0.00	20/03/1997	2500

at a few pivot-wavelengths, and then integrates the flux difference with respect to this continuum in the defined wavelength windows (Table 3) to determine the EWs. The pivot wavelengths used in this work are based on the same as those used by the above authors; these were chosen to avoid regions of strong emission or absorption features (Table 2). Four point flux values (3784, 3814, 3866, 3918 Å) were used for the Balmer discontinuity. The use of a compatible set of pivot points and wavelength windows is important, since it allows a detailed quantitative analysis of the stellar population by the synthesis techniques using the spectral library of star clusters (Bica & Alloin 1986).

The determination of the continuum was done interactively, was taking into account the flux level, noise and small uncertainties in wavelength calibration, as well as the presence of emission lines. The 5870Å point, in particular, is sometimes buried underneath the HeI 5876Å emission line. In such cases, adjacent wavelength regions guided the placement of the continuum. The final measured fluxes, normalized to the flux at 5870Å, are given in Table 2. After fitting the continuum points to a continuum spectrum, we measured the equivalent widths of seven characteristic absorption lines. When a noise spike was present in the wavelength window, it was necessary to make ‘cosmetic’ corrections. The results are given in Table 3. The first two rows give the names of the spectral lines and corresponding wavelength range. The EWs are in units of Å, and negative sign denotes emission lines.

#### 4. Stellar Population Synthesis

To study the history of star formation, age, and ionization mechanism of BCGs, we applied the synthesis method of Schmitt et al. (1996) for a determination of the stellar population in their nuclear region. In this method, we start with a sample of star clusters, consists of 3 clusters in the SMC, 12 in the LMC, 41 Galactic globular clusters and 3 rich compact Galactic open cluster, together with 4 HII regions (Bica & Alloin 1986). Then a grid of base components (comprising the values of the continuum at se-

lected points and of the EWs of selected absorption lines) is constructed by interpolation and extrapolation in the Age –  $[Z/Z_\odot]$  plane of those quantities of the clusters of the sample. The grid consists of 34 points with ages at  $10^7, 5 \times 10^7, 10^8, 5 \times 10^8, 10^9, 5 \times 10^9$ , and  $> 10^{10}$ yr, and  $[Z/Z_\odot] = 0.6, 0.3, 0.0, -0.5, -1.0, -1.5, -2.0$ , plus one point representing the HII region. The method, when applied to a given target, consists of adjusting the percentage contributions of the 35 base components by minimizing the difference between the resulting and measured EWs of the selected set of absorption lines. When all the resulting EWs reproduce those of the galaxy within allowed limits, we said to have obtained an acceptable solution. We then take all the acceptable solutions to form an average solution (Schmitt et al. 1996).

The computation can be performed in two ways: one way spans the whole Age –  $[Z/Z_\odot]$  plane (multi-minimization procedure, hereafter MMP), while the other is restricted to chemical evolutionary paths through the plane (direct combination procedure, hereafter DCP). We combine these two methods in our paper. We first use the MMP method to single out the main contributing components. And then, based on their resemblance to the whole-plane solution and on their reduced chi-square ( $\chi^2$ ), we select the best evolutionary path and use the DCP method to give the final result.

##### 4.1. The results of MMP

A detailed analysis of the MMP method can be found in Schmidt et al. (1989). This method searches the vector space of resolutions generated by the entire 35 component basis, leading to a representative set of acceptable solutions to the synthesis problem. We tried various combinations of the 35 components until a good match between the equivalent widths of the synthetic and observed lines is obtained. An iterative optimization procedure was used, and each iteration alters the percentages of different components. The input parameters are the measured equivalent

**Table 2.** Continuum points  $F_\lambda$  relative to  $F_\lambda(5870\text{\AA})$ , corrected for the foreground reddening

Name	$F_{3660}$	$F_{3784}$	$F_{3814}$	$F_{3866}$	$F_{3918}$	$F_{4020}$	$F_{4570}$	$F_{4630}$	$F_{5313}$	$F_{6630}$
IC1586	1.025	1.193	0.996	1.268	1.399	1.311	1.206	1.231	1.045	0.959
NGC2537	0.622	0.563	0.739	0.686	0.935	0.891	0.985	1.023	0.907	0.796
MRK19	1.255	1.189	1.933	2.758	2.201	1.790	1.314	1.249	0.989	0.866
MRK108	1.108	0.868	2.224	2.207	1.840	1.895	1.041	1.039	0.847	0.886
MRK25	1.100	1.113	1.215	1.394	1.378	1.338	1.206	1.206	1.089	0.870
MRK35	1.365	1.078	1.244	1.445	1.559	1.776	1.346	1.338	1.114	0.865
NGC4194	0.764	0.776	0.921	1.154	0.957	1.026	0.900	0.922	0.962	0.964
UGC9560	1.277	1.538	1.664	1.901	1.843	1.613	1.417	1.295	0.975	0.829
UGCA410	0.827	1.422	1.588	1.798	1.540	1.269	1.153	1.114	1.026	0.966
MRK499	1.012	1.331	1.216	1.442	1.551	1.440	1.252	1.252	1.033	0.935

**Table 3.** Measured equivalent widths in  $\text{\AA}$  for blue compact galaxies.

Galaxy Name	KCaII 3908-3952	H $\delta$ 4082-4124	CN 4150-4214	$G_{band}$ 4284-4318	H $\gamma$ 4318-4364	H $\beta$ 4846-4884	MgI+MgH 5156-5196
IC1586	5.845	0.287	-2.73	2.122	-0.89	-6.90	1.029
NGC2537	18.96	2.293	5.692	3.329	-14.7	-33.9	4.270
MRK19	9.878	5.313	-0.37	3.786	-4.21	-35.5	4.138
MRK108	18.25	-8.92	8.427	4.192	-37.1	-105.	3.434
MRK25	4.318	3.482	3.954	2.682	-2.39	-8.96	2.895
MRK35	2.769	-6.29	7.278	1.936	-15.1	-22.6	3.375
NGC4194	3.707	1.261	0.449	1.919	-2.62	-10.1	3.226
UGC9560	4.736	-4.67	4.230	3.678	-10.7	-40.5	4.303
UGCA410	10.61	1.073	14.33	8.688	-13.0	-50.6	3.237
MRK499	3.687	3.092	-1.07	0.960	4.124	-1.11	1.161

lent widths of the selected absorption lines, the continuum ratios and a set of trial values of  $E(B - V)$  between 0.0 and 1.0 at steps of 0.02. The result is expressed with the flux fractions at 5870 $\text{\AA}$  for each component. The flux fractions of different components for the 10 BCGs are shown in Table 4 (HII denotes the HII region component).

From the results of the MMP method, we find some obvious trends for all the BCGs. First, the dominant population are young ( $T \leq 5 \times 10^8 \text{yr}$ ) stellar clusters. Second, there is a small population of old ( $T > 10^{10} \text{yr}$ ) and high metallicity ( $[Z/Z_\odot] \geq 0$ ) globular clusters. Within old globular clusters low metallicity components contribute more than high metallicity components. Third, for the young and intermediate age ( $T \sim 10^9 - 5 \times 10^9 \text{yr}$ ) clusters, components with metallicities below or equal to the solar value make a large contribution. It shows that the stars in the BCGs have low metallicities, and this is consistent with our previous knowledge. Lastly, the younger components show a large dispersion in the plane, with no clear evolutionary paths. This could be due to the fact we have only used spectral data in the visible range. Additional data in the near ultraviolet and infrared will produce better-constrained solutions in the plane. Neverthe-

less, the presence of starbursts with  $T \approx 5 \times 10^8 \text{yr}$  is easily recognized from the MMP results.

#### 4.2. The results of DCP

To reduce the dispersion in metallicity, all the population synthesis so far made assumed some arbitrarily chosen chemical evolution path in the Age -  $[Z/Z_\odot]$  plane. The improvement in the method of this paper is: we shall pick out from the MMP results those components that contribute most importantly and use them to define paths of chemical evolution, thus reducing the degree of arbitrariness. The 3 bright BCGs appear to follow a path containing the 11 components along the time sequence  $T = 10^7 \sim 5 \times 10^9 \text{yr}$  at fixed metallicity  $[Z/Z_\odot] = -0.5$ , the metallicity sequence  $[Z/Z_\odot] = -0.5 \sim -2.0$  with  $T > 10^{10} \text{yr}$ , and the HII region. The 7 BCDGs follow a path containing the 12 components along the time sequence  $T = 10^7 \sim 5 \times 10^9 \text{yr}$  at fixed metallicity  $[Z/Z_\odot] = 0.0$ , the metallicity sequence  $[Z/Z_\odot] = 0.0 \sim -2.0$  with  $T > 10^{10} \text{yr}$ , and the HII region. In addition, we also tested other possible paths with different maximum metallicities; we found that the  $\chi^2$  of the path selected from MMP is the smallest.

**Table 4.** Flux fractions (%) at 5870Å for the whole plane solution for BCGs.

HIIR	E7	5E7	E8	5E8	E9	5E9	> E10	[Z/Z <sub>⊙</sub> ]	HIIR	E7	5E7	E8	5E8	E9	5E9	> E10
a) IC1586									b) NGC2537							
	2.37	0.45	0.45	0.00	0.00	0.00	0.00	0.6		1.00	0.06	1.36	2.99	2.52	1.23	0.04
	1.05	0.45	0.45	0.00	0.00	0.00	0.00	0.3		0.90	0.92	1.16	3.81	3.65	1.06	0.13
	2.30	0.45	0.45	0.00	0.00	0.00	0.00	0.0	0.00	0.75	5.79	5.02	10.1	11.5	6.34	1.11
3.36	6.43	2.08	2.04	14.6	0.00	0.00	0.00	-0.5		0.62	0.16	0.40	2.22	3.04	2.53	3.33
					0.76	0.61	0.61	-1.0						4.96	5.46	4.39
						4.72	6.22	-1.5							4.61	4.57
							50.1	-2.0								3.24
c) MRK19									d) MRK108							
	0.10	1.84	2.33	8.63	1.29	0.00	0.00	0.6		0.00	0.14	0.21	13.5	1.84	0.28	0.00
	0.10	1.08	3.54	10.3	1.74	0.00	0.00	0.3		0.00	0.00	0.07	14.1	1.90	1.21	0.00
0.00	0.16	4.78	5.97	26.8	6.49	0.13	0.26	0.0	0.00	0.00	0.14	0.28	31.7	9.10	2.13	0.70
	0.16	1.78	2.61	0.13	1.82	0.43	0.40	-0.5		0.00	0.00	0.14	0.00	1.69	1.56	0.78
					3.34	1.19	1.33	-1.0						4.18	2.27	4.68
						3.11	3.94	-1.5							3.69	4.68
							4.17	-2.0								2.63
e) MRK25									f) MRK35							
	0.16	0.68	1.05	3.74	2.48	0.67	0.02	0.6		0.34	3.33	3.28	3.98	0.27	0.00	0.00
	0.17	1.76	1.10	4.68	2.14	1.09	0.34	0.3		1.47	3.10	2.72	3.84	1.99	0.07	0.16
23.7	0.20	2.74	7.11	10.8	7.00	1.71	0.85	0.0	22.2	4.93	11.0	10.6	12.1	2.59	0.97	0.20
	0.24	1.66	2.85	0.53	1.31	1.64	1.63	-0.5		1.23	2.20	3.87	0.00	0.03	0.00	0.00
					2.88	1.77	1.93	-1.0						0.30	0.00	0.00
						2.24	3.20	-1.5							0.57	0.39
							3.94	-2.0								0.31
g) NGC4194									h) UGC9560							
	4.50	2.63	2.64	0.12	0.02	0.03	0.30	0.6		1.90	1.03	0.72	1.82	1.66	1.25	0.27
	4.79	3.29	3.40	0.34	0.12	0.11	0.50	0.3		1.23	1.27	1.98	1.73	1.73	2.02	0.27
	5.20	4.04	4.04	0.80	0.35	0.33	0.84	0.0	28.2	4.87	6.35	3.84	6.72	9.99	7.77	0.31
10.3	6.02	5.75	5.73	3.71	1.68	1.61	1.96	-0.5		1.84	1.02	1.28	0.57	2.78	1.59	0.8
					3.17	3.02	3.07	-1.0						0.94	0.76	0.71
						4.59	4.40	-1.5							0.23	0.25
							6.42	-2.0								0.16
i) UGCA410									j) MRK499							
	0.45	0.70	0.35	0.00	3.20	0.00	0.00	0.6		2.06	1.69	1.67	0.00	0.00	0.00	0.00
	1.68	0.44	0.00	4.08	1.15	0.00	0.00	0.3		2.47	2.07	1.75	0.00	0.00	0.00	0.00
0.45	9.39	2.47	0.03	21.9	10.1	1.36	0.00	0.0		4.21	5.15	5.04	0.00	0.00	0.00	0.00
	3.85	0.62	0.03	1.24	4.45	0.78	0.48	-0.5	6.30	10.3	8.53	8.25	1.62	0.00	0.00	0.00
					8.33	2.52	1.78	-1.0						0.00	0.00	0.00
						4.45	4.54	-1.5							1.95	3.04
							8.18	-2.0								33.9

Table 5 reports the path solution. The numbers of acceptable solutions and corresponding reduced chi-squared ( $\chi^2$ ) are also given. There is a great similarity between the path (DCP) and the whole plane (MMP) solution. Table 5a, 5g, 5j provide the results for the 3 bright BCGs (IC1586, NGC4194 and MRK499). We see that the younger components with age  $10^7 - 10^8$ yr make an appreciable contribution,  $\geq 35\%$ . The old globular clusters make even larger contributions. The intermediate-age components are small. The other tables in Table 5 provide the results for the 7 BCDGs. The dominant stellar components ( $> 30\%$ ) are in the young age bins ( $T \leq 5 \times 10^8$ yr).

The old globular clusters have different values in different galaxies; in some, lower than 10%, and in others as much as 35%. The BCDGs differ from the bright BCGs in two obvious aspects. First, the intermediate age components in the BCDGs amount to 20%, higher than in the bright BCGs. A peak occurs at about  $5 \times 10^8$ yr, which indicates that an enhanced star formation event occurred at that epoch. Second, the youngest components ( $T = 10^7$ yr) in the BCDGs are much lower than in the bright BCGs; probably indicating that the star formation rate of BCDGs is lower now. The HII region component is a featureless continuum, which acts in the synthesis as a dilutor of ab-

sorption lines. From Table 5, we note that some BCDGs have large contributions from the young components indicating intense star formation, and small contribution from HII regions, which suggests that intense starbursts have converted most gas into stars.

## 5. Synthesized Spectra

We now display the results of stellar population synthesis in a more visible form in Figure 1. OBS represents the observed spectrum of galaxy (OBS+5, the +5 indicating that it is displaced upwards by 5 units). SYN represents the synthetic spectrum resulting from the percentage contribution in Table 5. The various stellar components are designated as follow. OGC stands for the contribution from the old globular cluster ( $T > 10^{10}\text{yr}$ ); IYC for the contribution from the intermediate age star cluster ( $T \sim 10^9 - 5 \times 10^9\text{yr}$ ); YBC for the contribution from the young blue star clusters ( $10^7 \leq T \leq 5 \times 10^8\text{yr}$ ), and HII stands for the contribution from HII regions. The emission line spectrum (OBS-SYN) resulting from subtracting SYN from OBS, is shown in the lower part of figure.

The figure shows that the synthesized spectrum gives a good fit to the observed continuum and absorption lines for each galaxy. We can conclude that the continuum of BCGs comes both from the stars (particularly the young and intermediate-age stars) and HII regions. It may be interpreted that the main energy sources of BCGs are young hot O, B stars, which lead to the formation of HII regions around them.

The stellar subtracted spectra (OBS-SYN) can be used to study the emission lines. We have measured the main strong emission line intensities with Gaussian fits. The results, relative to that of  $\text{H}\alpha$  are shown in Table 6. At this stage our spectra are corrected for the foreground reddening and the internal reddening from the stellar populations (see next section). First, we have used the  $\text{H}\alpha/\text{H}\beta$  ratio in Table 6 to derive the internal reddening value associated with the line-emitting regions. It will be calculated in next section. Second, we have attempted to identify the ionizing mechanism in these nuclei, using the emission line ratios in the visible region.

We compared emission-line ratios calculated from Table 6 with the diagnostic diagram  $[\text{NII}]\lambda 6584/\text{H}\alpha - [\text{OII}]\lambda 3727/[\text{OIII}]\lambda 5007$  from Baldwin, Phillips & Terlevich (1981). We plot the results in Figure 2. From this figure, we find that the BCGs are always located near or within the HII region. None of them are located in the loci of planetary nebulae, power-law, or shock-heated region. This result indicates that the young, massive mass stars formed in the nucleus are heating the gas in the nucleus of BCGs. This result is very similar to those found from population synthesis. We also show in this diagram the effect of internal reddening. We can see that it, even in the case of NGC4194, with the strongest reddening derived from its line-emitting regions, is not large.

## 6. Results

From the stellar population analysis in Sect. 4 and the emission line spectrum in Sect. 5, combined with results from other studies, it is now possible to reveal some global properties of BCGs.

### 6.1. Age and Star Formation Rate

There are two major competing theories for BCGs. The first one claims that BCGs are truly young systems undergoing the first star formation episode in the galaxy's lifetime. The second model suggests that BCGs are old galaxies, which are mainly composed of older stellar populations, with, however, a brief episode of violent star formation, in order to account for the observed spectroscopic features and spectral energy distributions.

Using the population synthesis method, we know the stellar population (different ages and metallicities) percentage contributions at  $\lambda = 5870\text{\AA}$  for each of the 10 BCGs. These results show clearly that, for each, the old globular clusters and intermediate age components ( $T \leq 10^9\text{yr}$ ) make sizeable contributions to the galactic spectrum. The presence of large fractions of old or intermediate age components indicates that the star formation happened already at an early stage, and at a high rate. Our results support the second model that BCGs are old galaxies.

For IC1586, NGC4194 and MRK499, the contributions coming from the young and the old stellar components are large, but that from the intermediate age component is small. It suggests that the rate of star formation during the intermediate age period is smaller than in the other periods, and the star formation process is not continuous in these galaxies. For the BCDGs, the contribution from the intermediate age component is important, star formation was most vigorous in its intermediate age period, with relatively small contributions from the other periods. This also implies that star formation in these galaxies is also discontinuous.

The other result of our population synthesis is that while the observed properties of the bright BCGs (IC1586, NGC4194, MRK499) and the BCDGs are very similar, their stellar components and star formation regimes are generally different. There are many old and young stellar components in bright BCGs, and its recent star formation rate is very high. For BCDGs, the old and young stellar components are relatively small, but the contribution from intermediate age stellar populations is important.

The stellar population synthesis suggests that BCGs are old galaxies, in which the process of star formation is intermittent. Star formation has been violent in one of its evolution periods. These results are also supported by other observations (Papaderos et al. 1996, Sung et al. 1998, Aloisi et al. 1999). It illustrates that the present method is more than a simple population synthesis since

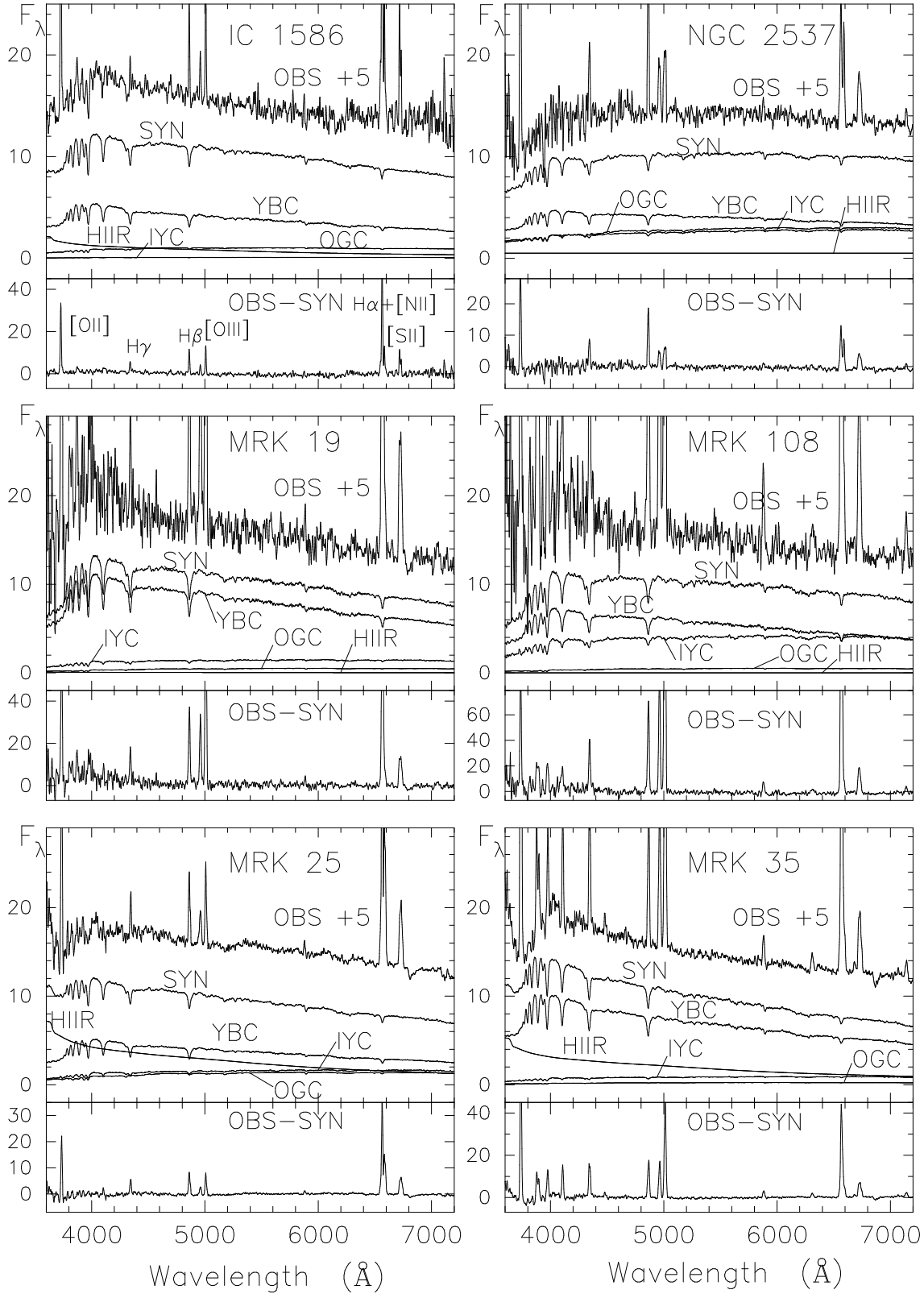


**Fig. 1.** Observed spectra for our 10 BCGs are shown together with the best-match population synthesis models (cf. Table 5). The observed galaxy spectrum (OBS) has been corrected for the foreground reddening  $E(B-V)_G$  and shifted by 5 units. In the synthetic spectrum (SYN), the young population (YBC) dominates the light, but the intermediate age component (IYC) is also important. The emission line spectrum appears in the (OBS-SYN) difference, in the lower part of the figure. OBS and SYN are normalized to  $F_\lambda = 10$  at  $5870\text{\AA}$ .

**Table 5.** Flux fractions (%) at 5870Å for the best path solution of BCGs.

HIIR	E7	5E7	E8	5E8	E9	5E9	> E10	$[Z/Z_{\odot}]$	HIIR	E7	5E7	E8	5E8	E9	5E9	> E10
a) IC1586 : Acceptable Solutions: 78, $\chi^2 = 1.23$									b) NGC2537: Acceptable Solutions: 75, $\chi^2 = 1.08$							
								0.6								
								0.3								
								0.0	0.02	2.73	5.75	6.29	26.3	15.2	9.54	4.37
5.69	7.57	4.72	4.81	18.8	0.52	0.41	0.48	-0.5								7.62
								-1.0								8.31
								-1.5								7.87
								-2.0								5.99
c) MRK19 : Acceptable Solutions: 143, $\chi^2 = 1.30$									d) MRK108: Acceptable Solutions: 93, $\chi^2 = 0.87$							
								0.6								
								0.3								
								0.0	0.00	0.86	3.66	3.66	44.1	32.4	10.0	2.47
0.25	1.81	8.93	12.2	52.4	10.7	4.24	2.67	-0.5								1.40
								-1.0								1.08
								-1.5								0.21
								-2.0								0.21
e) MRK25: Acceptable Solutions: 133, $\chi^2 = 1.12$									f) MRK35: Acceptable Solutions: 106, $\chi^2 = 0.73$							
								0.6								
								0.3								
								0.0	16.5	8.57	21.9	21.1	18.6	7.49	2.80	0.61
22.5	2.10	7.17	9.40	19.8	12.1	6.70	3.87	-0.5								0.73
								-1.0								0.94
								-1.5								0.47
								-2.0								0.41
g) NGC4194: Acceptable Solutions: 54, $\chi^2 = 1.03$									h) UGC9560: Acceptable Solutions: 52, $\chi^2 = 0.55$							
								0.6								
								0.3								
								0.0	29.5	4.28	8.01	7.26	15.0	14.7	11.4	3.69
18.5	7.90	5.53	5.47	20.2	2.36	2.72	4.39	-0.5								2.47
								-1.0								1.72
								-1.5								1.16
								-2.0								0.73
i) UGCA410: Acceptable Solutions: 95, $\chi^2 = 0.86$									j) MRK499 : Acceptable Solutions: 151, $\chi^2 = 0.53$							
								0.6								
								0.3								
								0.0								
								-0.5	5.28	17.3	19.9	19.3	3.70	0.51	0.30	0.31
9.99	0.66	2.63	2.30	28.5	19.3	6.16	0.93	-1.0								1.41
								-1.5								5.19
								-2.0								26.8

it provides a direct estimate of the chemical evolution of the galaxy.

### 6.2. Internal Reddening

When we investigate the internal energy source, physical condition and internal structure of galaxies, we must take into account the effect of internal reddening (Pizagno & Rix 1998). The effect of dust extinction on the emerging radiation is one of the least understood physical phenomena (Calzetti 1997, Ho et al. 1997). To study the internal reddening properties of BCGs, we quantify the

discrepancy between the dust extinction measured from the emission line ratios and the optical continuum.

In the method of population synthesis used in this paper, the internal reddening is taken as an adjustable parameter, so that an estimate for the internal reddening is made at the same time as the stellar composition. We try various values of the internal reddening, make the appropriate correction in the continuum spectrum, then use this corrected continuum spectrum in the synthesis to find the best solution. This is an empirical way of determining the galactic reddening, its advantage is that it is assumption-free. The values of galactic internal reddening are listed



**Table 6.** Emission line intensities with respect to  $H\alpha$  (normalized to 100) and the internal reddening value of BCGs.

Galaxy Name	[OII]	H $\gamma$	H $\beta$	[OIII]	[OIII]	[NII]	[SII]	$X^*$	$Y^{**}$	E(B-V)		
	3727	4340	4861	4959	5007	6584	6717,31			H $\alpha$ /H $\beta$	MMP	DCP
IC1586	65.62	11.29	20.15	10.00	23.22	16.83	36.47	0.45	-0.77	0.51	0.13	0.14
NGC2537	185.29	45.84	104.32	34.37	56.40	59.05	66.29	0.52	-0.23		0.13	0.12
MRK19	52.61	11.95	28.09	24.12	78.23	7.08	23.18	-0.17	-1.15	0.20	0.03	0.03
MRK108	26.19	11.87	24.18	32.45	104.44	2.09	11.22	-0.60	-1.68	0.34	0.03	0.03
MRK25	71.44	16.36	29.08	12.85	25.32	59.58	37.77	0.45	-0.22	0.17	0.06	0.04
MRK35	141.15	31.25	37.82	37.81	99.38	24.01	23.55	0.15	-0.62		0.05	0.04
NGC4194	20.77	5.24	15.63	4.73	14.58	48.59	24.84	0.15	0.31	0.75	0.33	0.35
UGC9560	67.07	9.32	26.21	3.19	108.70	10.84	15.68	-0.21	-0.96	0.27	0.03	0.02
UGCA410	28.25	9.15	26.77	47.21	159.02	7.61	13.01	-0.75	-1.12	0.25	0.02	0.02
MRK499	54.83	8.91	21.23	19.84	49.43	25.50	20.00	0.04	-0.59	0.46	0.15	0.16

\* $X \equiv \log([\text{OII}]\lambda 3727/[\text{OIII}]\lambda 5007)$ ; \*\* $Y \equiv \log([\text{NII}]\lambda 6584/H\alpha)$ .

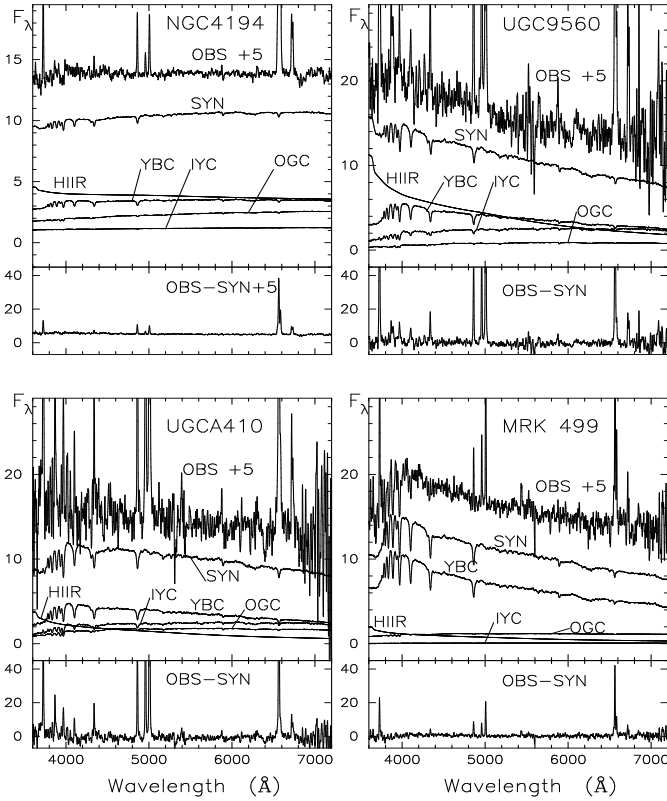
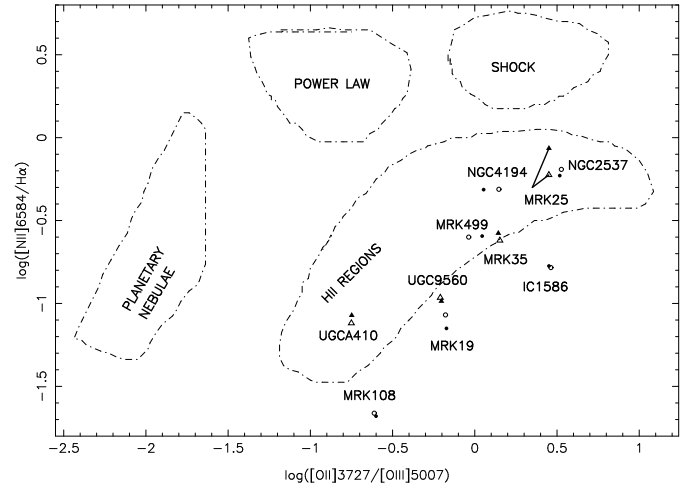


Fig.1 continue.

in Table 6,  $E(B - V)_{\text{MMP}}$  is the result from the MMP method,  $E(B - V)_{\text{DCP}}$  is the result from the DCP method. We find that the values are small ( $E(B - V) \leq 0.35$ ), which is consistent with the BCGs being metal-poor and dust-poor. We find the reddening also clearly depends on the shape of the spectrum. The flattest spectrum (NGC4194) goes with the largest color excess. The steeper spectrum, the less the extinction.

The Balmer line ratio  $H\alpha/H\beta$  allows us to characterize the dust extinction in the regions where the nebular



**Fig. 2.** Logarithmic plot of the line intensity ratios  $[\text{NII}]\lambda 6584/H\alpha$  versus  $[\text{OII}]\lambda 3727/[\text{OIII}]\lambda 5007$ . Open symbols correspond to data corrected for the foreground reddening. Black symbols represent data points with an additional reddening correction intrinsic to the line emitting regions.

lines are produced. We measured the internal reddening value  $E(B - V)_{H\alpha/H\beta}$  of the 10 BCGs using the observed emission lines  $H\alpha$  and  $H\beta$ . The difference in the calculation of  $E(B - V)_{H\alpha/H\beta}$  between the previous work and ours is that we can correct the underlying stellar absorption  $EW_{\text{abs}}$  from the results of stellar population synthesis without making any hypotheses. The result of  $E(B - V)$  is listed in the last 3 columns of Table 6.

From this table, we can find that the internal reddening of the stellar continuum in BCGs is generally lower than that of ionized gas. A model of foreground dust clumps, with different covering factors for gas and stars, is a possible explanation for the difference. The covering factor by dusty clumps is greater for the gas region that generates the emission lines than for the stars that produce the continuum. That the continuum emission of stars is less

obscured than are the emission lines of ionized gas, has been pointed out for other kinds of emission line galaxies (Calzetti et al. 1994).

## 7. Summary

We have observed the optical spectra for the nuclear regions of 10 blue compact galaxies. We have studied their stellar populations by matching the spectra of these objects to a library of integrated spectra of star clusters. Our conclusions can be summarized as follows.

The quantitative analysis indicates that the nucleus of the 3 bright BCGs is dominated by young components and the star-forming process is still ongoing. The maximum metallicity of the stellar population is  $[Z/Z_{\odot}] = -0.5$ . The nucleus of the dwarf BCGs (BCDGs, which have  $M_B > -20$ ), on the other hand, is dominated by the intermediate age component. The metallicity has, at most, reached up to the solar value. The young component is not so important as in the bright BCGs, but it is still not negligible.

For all BCGs, the old population in the range  $[Z/Z_{\odot}] \leq 0.0$  is important, the very metal-rich component provides quite a small contribution in these galaxies. The stellar populations of BCGs suggest that they are old galaxies with intermittent star formation history.

A good match can be achieved between the synthesized and observed spectrum of BCGs. It suggests that the stellar radiation is an important energy source for BCGs.

The emission-line spectra from the gaseous components in these objects were isolated and analyzed. Using these stellar subtracted spectra, we have calculated the internal reddening value of the emission line regions and attempted to identify the ionizing mechanism in BCGs. Comparing with the reddening derived from the continuum, we conclude that the continuum and emission line regions have different degrees of dust obscurations.

The stellar subtracted spectra should be very useful for further investigation of physical conditions and chemical abundance of the emission line regions of BCGs.

*Acknowledgements.* We are grateful to the Chinese 2.16m Telescope time allocation committee for their support of this programme and to the staff and telescope operators of the Xinglong Station of Beijing Astronomical Observatory for their support. Especially we would like to thank Prof. J.Y. Hu and Dr. J.Y. Wei for their active cooperation which enable all of the observations to go through smoothly. We are also deeply grateful to Henrique R. Schmitt for kindly providing us the procedure of stellar population synthesis. We also thank the anonymous referee for helpful comments and constructive suggestions. Special Thanks to Dr. S. Mao and Dr. T. Kiang for their hard work of English revision of this paper. This work was supported by grants from the National Pandem Project and Natural Science Foundation of China.

## References

- Aloisi A., Tosi M., & Greggio L., 1999, AJ 118, 302  
 Baldwin J. A., Phillips M.M., Terlevich R., 1981, PASP 93, 5  
 Bica E., 1988, A&A 195, 76  
 Bica E., Alloin D., 1986, A&A 166, 83  
 Bica E., Alloin D., Schmitt H.R., 1994, A&A, 283, 805  
 Bonatto C. J., Pastoriza M. G., Alloin D., et al., 1998, A&A 334, 439  
 Burstein D., Heiles C., 1984, ApJS 54, 33  
 Calzetti D., 1997, AJ 113, 162  
 Calzetti D., Kinney A. L., Storchi-Bergmann T., et al., 1994, ApJ 429, 582  
 Cid Fernandes R., Storchi-Bergmann T., Schmitt H.R., 1998, MNRAS 297, 579  
 Conti P. S., 1991, ApJ 377, 115  
 Doublier V., Comte G., Petrosian A., et al., 1997, A&AS 124, 405  
 Fanelli M. N., O'Connell R. W., Thuan T. X., 1988, ApJ 334, 665  
 Garnett D., Skillman E.D., Dufour R.J., et al., 1997, ApJ 481, 174  
 Gondhalekar P. M., Johansson L.E.B., Brosch N., et al., 1998, A&A 335, 152  
 Grebel E. K., 1999, eds. P. Whitelock & R. Cannon, in IAU Symp. 192, p.17  
 Ho L. C., Filippenko A. V., Sargent W.L.W., 1997, ApJ 487, 579  
 Hunter D. A., Thronson JR. H. A., 1995, ApJ 452, 238  
 Izotov Y.I., Thuan T.X., 1999, ApJ 511, 639  
 Izotov Y.I., Thuan T.X., Lipovetsky V.A., 1994, ApJ 435, 647  
 Izotov Y.I., Thuan T.X., Lipovetsky V.A., 1997, ApJS 108, 1  
 Jablonka P., Alloin D., Bica E. 1990, A&A 235, 22  
 Kinney A. L., Bohlin R. C., Calzetti D., et al., 1993, ApJS 86, 5  
 Krüger H., Fritze-von Alvensleben U., Loose H. -H., 1995, A&A 303, 41  
 Lipovetsky V.A., Chaffee F.H., Izotov Y.I., et al., 1999, astro-ph/9902368  
 Martin C. L., 1998, ApJ 506, 222  
 Mas-Hesse J. M., Kunth D., 1998, A&A astro-ph/9812072  
 McQuade K., Calzetti D., Kinney A. L., 1995, ApJS 97, 331  
 Östlin G., Amram P., Masegosa J., et al., 1999, A&AS 137, 419  
 Pizagno J., Rix H.W., 1998, AJ 116, 2191  
 Papaderos P., Loose H.-H., Fricke K.J., et al., 1996, A&A 314, 59  
 Sage L. J., Salzer J. J., Loose H. H., 1992, A&A 265, 19  
 Salzer J. J., Norton S. A., 1999, astro-ph/9810338  
 Sargent W.L.W., Searle L., 1970, ApJ 162, L115  
 Schmidt A. A., Bica E., Dottori H., 1989, MNRAS 238, 925  
 Schmitt H. R., Bica E., Pastoriza M. G., 1996, MNRAS 278, 965  
 Storchi-Bergmann T., Kinney A. L., Challis P., 1995, ApJS 98, 103  
 Sung E. C., Han C., Ryden B. S., Patterson R., et al., 1998, ApJ 505, 199  
 Thuan T.X., Izotov Y.I., Lipovetsky V.A., 1995, ApJ 445, 108  
 Thuan T.X., Izotov Y.I., Lipovetsky V.A., 1996, ApJ 463, 120  
 van Zee L., Westpfahl D., Haynes M. P., et al., 1998, AJ 115, 1001  
 Vaceli M. S., Viegas S.M., Gruenwald R., et al., 1997, AJ 114, 1345